Journal of Fluids and Structures (1999) **13,** 481–498
Article No.: jfls. 1999.0217, available online at http://www idealibrary.com on IDEAL

ON THE COMPRESSION WAVE GENERATED WHEN A HIGH-SPEED TRAIN ENTERS A TUNNEL WITH A FLARED PORTAL

M. S. Howe

Boston University, College of Engineering, 110 Cummington Street
Boston MA 02215, U.S.A.

(Received 2 June 1998 and in revised form 2 March 1999)

An analysis is made of the compression wave generated when a high-speed train enters a tunnel with a flared portal. Nonlinear steepening of the wavefront in a very long tunnel is responsible for an intense, environmentally harmful, *micro-pressure wave*, which propagates as a pulse from the distant tunnel exit when the compression wave arrives, with amplitude proportional to the maximum gradient in the compression wavefront. The compression wave profile can be determined analytically for train Mach numbers M satisfying $M^2 \ll 1$, by regarding the local flow near the tunnel mouth during train entry as *incompressible*. In this paper, the influence of tunnel portal flaring on the initial thickness of the compression wave is examined first in this limit. The shape of the flared portal is "optimal" when the *pressure gradient* across the front is constant and an overall minimum, so that the pressure in the wavefront increases *linearly*. This linear behaviour is shown to occur for a flared portal extending a distance ℓ into the tunnel from the entrance plane ($x = 0$) only when the tunnel cross-sectional area $S(x)$ satisfies

$$\frac{S(x)}{\mathscr{A}} = \frac{1}{[\mathscr{A}/\mathscr{A}_E - (x/\ell)\,(1 - \mathscr{A}/\mathscr{A}_E)]}, \quad -\ell < x < 0,$$

where x increases negatively with distance into the tunnel, $\mathscr{A}$ is the cross-sectional area in the uniform section of the tunnel ($x < -\ell$), and $\mathscr{A}_E$ is the tunnel entrance cross-section. The optimum portal is achieved by adjusting the value of $\mathscr{A}/\mathscr{A}_E$ to make the pressure gradient continuous, and a formula is derived for this ratio for tunnels of semi-circular cross-section. For optimal flaring, the pressure rises linearly as the front of the train traverses the flared section of length ℓ, and the thickness of the compression wavefront $\sim \ell/M$.

A formula is proposed for extrapolating these predictions to train Mach numbers as large as 0·4, which is expected to be typical of future high-speed rail operations. It is validated for the special case of a circular cylindrical tunnel, for which an exact solution is known for arbitrary subsonic Mach numbers, and by comparison with scale model experiments using trains of various nose profiles.

1. INTRODUCTION

A TRAIN ENTERING A TUNNEL generates a compression wave that propagates into the tunnel at the speed of sound. On reaching the distant tunnel exit the wave emerges as a pressure pulse, the *micro-pressure wave*, whose amplitude and duration depend on train speed on entry, its cross-sectional area relative to the tunnel, and on the tunnel length (Iida *et al.* 1996; Maeda *et al.* 1993; Ozawa *et al.* 1991; Swarden & Wilson 1970; Ogawa & Fujii 1994a, 1996, 1997; Howe 1998a, b; Mestreau *et al.* 1993). The amplitude of the compression wave is usually of the order of 0·01 atm (~150 dB) for a train travelling at Mach numbers M exceeding about 0·2 (~250 kph), and the pressure rise occurs over a distance (the wavefront 'thickness') typically of order $D/M \sim 5$ tunnel diameters D. The strength of the micro-pressure wave is

0889–9746/99/040481 + 18 $30.00

proportional to the steepness of the compression wavefront at the tunnel exit, and for tunnels longer than about 3 km with modern concrete slab tracks (offering little dissipation to the propagating wave), nonlinear wave steepening can produce peak micro-pressure wave amplitudes of 50 Pa (≈ 128 dB) or more near the exit. This is comparable to the sonic boom from a supersonic aircraft, and frequently causes structural damage and much annoyance.

Nonlinear steepening is effectively suppressed by relaxation processes when the initial *rise time* of the wave is large (Ozawa *et al.* 1991), and can therefore be forestalled by designing the train nose profile and tunnel portal to make the initial thickness of the compression wave as large as possible. A sufficiently "slender" nose profile has been found to reduce the micro-pressure wave strength by about 3 dB (Iida *et al.* 1996; Maeda *et al.* 1993). Much larger reductions are obtained, however, by modifying the tunnel entrance geometry. In the case of adjacent, parallel tunnels, for example, the initial wave thickness is increased by allowing high-pressure air produced by an entering train to flow into the neighbouring tunnel through a suitable vent close to the entrance. But, the most significant attenuations are currently achieved (in Japan) by the installation of an entrance "hood". This extends up to 50 m ahead of the tunnel entrance, and produces a large increase in compression wave thickness by venting high-pressure air through "windows" distributed along the hood walls. A fivefold increase in wave thickness has been reported for a hood of length 49 m (Ozawa *et al.* 1991).

However, tunnel entrance hoods tend to be unsightly and there is a corresponding need to investigate alternative tunnel portal modifications for achieving comparable increases in the compression wave rise time. Portal "flaring" has long been considered ideal for this purpose (Ozawa *et al.* 1976; Vardy 1978; Ogawa & Fujii 1994b). The compression wave thickness will necessarily be very large if the flaring is gradual, and extends sufficiently far into the tunnel from the entrance plane, but may be impracticable if this requires the tunnel cross-section at the entrance to be too large.

In this paper, the theory of compression wave generation is discussed for a train entering a tunnel with a flared entrance. The initial compression wave profile is determined in terms of a Green's function tailored to the tunnel entrance geometry, and a distribution of monopole sources that represent the displacement of fluid by the advancing train. This can be done analytically for arbitrary portal geometry for train Mach numbers satisfying $M^2 \ll 1$ by the method of Howe (1998a). We show how these results can be extrapolated to encompass the higher Mach numbers ($\sim$0·4) encountered in modern high-speed operations. The extrapolation formula is justified by comparison with exact analytical predictions and with experiment for the special case of a "tunnel" formed by an unflanged circular cylinder.

The theory is applied to optimize the initial rise time when a section of the tunnel entrance of length ℓ is flared. When ℓ is prescribed, it is required to determine the functional dependence on position of the flared tunnel cross-section that maximizes the rise time and produces a *linear* pressure increase across the compression wavefront. Thus, the maximum wavefront thickness attainable by this means is $\sim \ell/M$. Nonlinearity would cause any other initial wave profile to become "rough", with regions where the pressure gradient becomes locally large, thereby favouring shock formation in a long tunnel. The optimum is shown to be achieved when the cross-section in the flared portal decreases inversely with distance into the tunnel from an appropriately chosen inlet area.

The theory of compression wave generation is formulated in Section 2. Green's function for a flared portal is derived in Section 3 for the case where $M^2 \ll 1$, and applied to determine the shape of an optimally flared portal. The extrapolation of predictions to higher Mach numbers is then discussed (Section 4), including a comparison with experimental data of Maeda *et al.* (1993). Numerical predictions are presented for Mach numbers extending up to

0·4 for various model train nose profiles that have been examined experimentally. The theory determines the *initial* profile of the compression wave ahead of the train, immediately after the interaction of the train nose with the portal. This profile can be used to define initial conditions for a nonlinear calculation of the subsequent propagation of the wave along the tunnel, but this is not pursued here.

2. REPRESENTATION OF THE COMPRESSION WAVE

Consider a train travelling at constant speed U in the negative x-direction into the flared entrance portal of a tunnel of semi-circular cross-section, with the origin O of the coordinate axes (x, y, z) taken at ground level at the centre of the tunnel entrance plane (Figure 1). An axial section of the tunnel extending a distance ℓ into the tunnel from the entrance is flared, with variable tunnel cross-sectional area $S(x)$, which satisfies

$$\begin{aligned} S(x) &= \mathscr{A} \equiv \frac{\pi}{2} R^2 = \text{constant}, \quad \text{for } x < -\ell, \\ S(0) &= \mathscr{A}_{\mathrm{E}} \equiv \frac{\pi}{2} R_{\mathrm{E}}^2. \end{aligned} \tag{2.1}$$

That is, $\mathscr{A}$ and R are respectively the constant cross-sectional area and radius in the uniform region $x < -\ell$, and $\mathscr{A}_{\mathrm{E}}$ and R_{E} are the corresponding values in the tunnel entrance plane.

The profiled nose (of length L) of the train is assumed to be sufficiently streamlined that the influence of flow separation on compression wave formation may be ignored. The displacement of fluid by the advancing train may then be represented by replacing the train by a system of constant strength volume sources (Howe 1998a, b) distributed within the envelope of the train, that translates with the train at speed U. The distribution of these sources at time t will be denoted by $q(x + Ut, y, z)$, where $q(\mathbf{x})$ is defined to be the source distribution at $t = 0$, when the front of the train will be supposed to pierce the tunnel entrance plane. The motion produced by the sources is irrotational, and can be expressed in terms of a velocity potential $\varphi(\mathbf{x}, t)$ determined by

$$\left(\frac{1}{c_{\mathrm{o}}^2}\frac{\partial^2}{\partial t^2} - \nabla^2\right)\varphi = -q(x + Ut, y, z), \tag{2.2}$$

where c_{o} is the speed of sound. φ is required to have outgoing wave behavior and satisfy the condition $\partial\varphi/\partial x_n = 0$ of vanishing normal velocity on the surfaces S consisting of the rigid

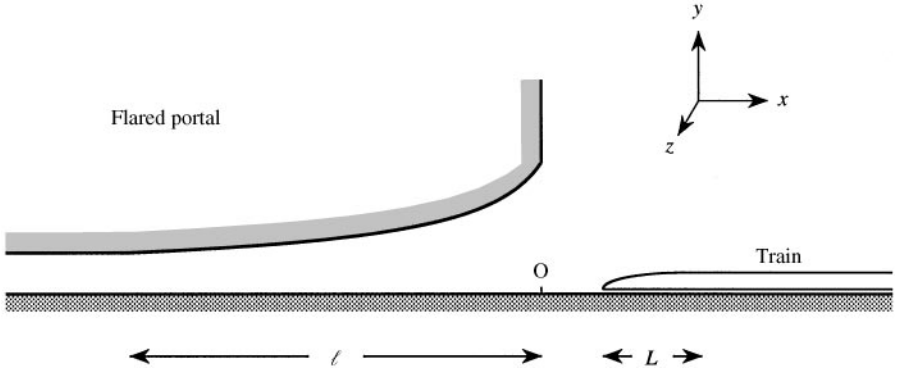

Figure 1. Schematic profile of flared tunnel entrance of length ℓ.

sections of the tunnel walls and the ground plane $y = 0$. Observe that, although the left-hand side of equation (2.2) is linear in φ, the motion described by the velocity potential in the neighbourhood of the train is fully nonlinear, and represents the massive displacement and compression of the fluid by the train on approaching and entering the tunnel. However, within the tunnel, ahead of the train, where the motion is dominated by the advancing compression wave of characteristic amplitude $\sim 0{\cdot}01$ atmos, the unsteady motion is well approximated by the *linearized* equations of motion, at least before wave steepening becomes important.

The solution of equation (2.2) can be expressed in the form

$$\varphi(\mathbf{x}, t) = -\iint G(\mathbf{x}, \mathbf{x}', t-\tau) q(x' + U\tau, y', z')\, \mathrm{d}^3\mathbf{x}'\, \mathrm{d}\tau, \tag{2.3}$$

where Green's function $G(\mathbf{x}, \mathbf{x}', t-\tau)$ has vanishing normal derivative $\partial G/\partial x_n'$ on S, and satisfies

$$\left(\frac{1}{c_o^2}\frac{\partial^2}{\partial \tau^2} - \nabla'^2\right) G = \delta(\mathbf{x} - \mathbf{x}')\delta(t-\tau), \quad G = 0 \quad \text{for } \tau > t, \tag{2.4}$$

where ∇'^2 is the Laplacian with respect to $\mathbf{x}'$ (Morse & Feshbach 1953). The integrations in equation (2.3) are over all time τ and the fluid volume.

A closed-form expression for $G(\mathbf{x}, \mathbf{x}', t-\tau)$ is available only for the highly simplified case of a tunnel modelled as a semi-infinite, thin-walled, unflanged cylinder of semi-circular cross-section (Howe 1998b). For train Mach numbers M less than about $0{\cdot}2$, the thickness of the compression wavefront $\sim d/M \gg d$, where d is a characteristic length of the tunnel portal: $d \sim 2R$ for a cylindrical tunnel of radius R. In these circumstances, when the wavelength of compressible motions greatly exceeds the tunnel diameter, $G(\mathbf{x}, \mathbf{x}'; t-\tau)$ can be approximated by the *compact* Green's function, which was shown by Howe (1998a) to be given by

$$G(\mathbf{x}, \mathbf{x}'; t-\tau) \approx \frac{c_o}{2\mathscr{A}} \{\mathrm{H}(t - \tau - |\phi^*(\mathbf{x}) - \phi^*(\mathbf{x}')|/c_o) - \mathrm{H}(t - \tau + (\phi^*(\mathbf{x}) + \phi^*(\mathbf{x}'))/c_o)\}, \tag{2.5}$$

where $\phi^*(\mathbf{x})$ is the velocity potential of an hypothetical incompressible flow *out* of the tunnel portal, normalized such that

$$\begin{aligned} \phi^*(x) &\approx x - \ell' \quad \text{as } x \to -\infty \quad \text{inside the tunnel,} \\ &\approx \mathscr{O}(1/|\mathbf{x}|) \quad \text{as } |\mathbf{x}| \to \infty \text{ outside the tunnel,} \end{aligned} \tag{2.6}$$

and $\mathrm{H}(x), = 0,\ 1$ according as $x \lessgtr 0$, is the Heaviside step function.

These formulae are applicable for any tunnel whose interior cross-sectional area is ultimately constant and equal to $\mathscr{A}$. The length $\ell' \sim \sqrt{\mathscr{A}}$ is the "end-correction" of the portal ($\approx 0{\cdot}61R$ for the semi-circular, cylindrical tunnel of radius R; Rayleigh 1926); the precise value is dependent on details of portal geometry. $\phi^*(\mathbf{x})$ varies continuously through the tunnel entrance, increasing from a large negative value when x is negative and large within the tunnel, to zero as $|\mathbf{x}| \to \infty$ outside the tunnel. It is numerically of order $\sqrt{\mathscr{A}}$ in the neighbourhood of the portal, where its rate of change depends on the entrance shape and its environment. The approximation (2.5) is uniformly valid when regarded as a function of either $\mathbf{x}$ or $\mathbf{x}'$ provided at least one of these points lies within the tunnel at a large distance compared to the tunnel diameter.

The solution (2.3) determines the *initial* compression wave profile, prior to the onset of nonlinear steepening, and is valid several tunnel diameters ahead of the train, during and just after tunnel entry. At such points the disturbed motion is small, and the perturbation

pressure p can be calculated from the linearized Bernoulli equation $p = -\rho_o \partial\varphi/\partial t$, where ρ_o is the undisturbed air density. This yields

$$p(\mathbf{x}, t) = \frac{\rho_o c_o}{2\mathscr{A}} \int \{q(x' + U[t] - M\phi^*(\mathbf{x}'), y', z') - q(x' + U[t] + M\phi^*(\mathbf{x}'), y', z')\}\, \mathrm{d}^3\mathbf{x}', \quad (2.7)$$

where $[t] = t + \phi^*(\mathbf{x})/c_o \approx t + (x - \ell')/c_o$ is the retarded time.

Here it is supposed that the observation point $\mathbf{x}$ is sufficiently far within the tunnel that $\phi^*(\mathbf{x}) \approx x - \ell'$, but that nonlinear steepening has not become significant. The subsequent propagation of the wave within a long tunnel could be calculated by using equation (2.7) to define the initial conditions for a nonlinear theory.

The source distribution q is nonzero only in the vicinities of the nose and tail of the train, where its cross-sectional area is changing. The compression wave is generated as the nose enters the tunnel, and for the purpose of calculating the contribution from the nose, the length of the train may be assumed to be so large that the rear end can be ignored. During the formation of the wave, and provided the train Mach number is small enough that terms $\sim \mathscr{O}(M^2)$ are negligible, the term $M\phi^*(\mathbf{x}')$ in the arguments of q in equation (2.7) is small, and

$$\begin{aligned} p \approx p(x, t) &= \frac{-\rho_o U}{\mathscr{A}} \int \phi^*(\mathbf{x}') \frac{\partial q}{\partial x'}(x' + U[t], y', z')\, \mathrm{d}^3\mathbf{x}' \\ &= \frac{\rho_o U}{\mathscr{A}} \int q(x' + U[t], y', z') \frac{\partial \phi^*}{\partial x'}(\mathbf{x}')\, \mathrm{d}^3\mathbf{x}' \end{aligned} \quad (2.8)$$

where the second line follows by integration by parts, and by recalling that $\phi^*(\mathbf{x}') \to 0$ outside the tunnel.

Predictions of this formula for a cylindrical, thin-walled tunnel have been compared (Howe 1998a) with data of Maeda *et al.* (1993) derived from model scale experiments involving the projection of wire-guided model trains into a circular cylindrical tube at $M \approx 0{\cdot}19$ when $\mathscr{A}_o/\mathscr{A} \approx 0{\cdot}116$, where $\mathscr{A}_o$ is the uniform cross-sectional area of the train to the rear of the profiled nose. Good agreement with experiment was obtained when the monopole distribution $q(\mathbf{x})$ was approximated by the *line source*

$$q(\mathbf{x}) = U\mathscr{A}_o Q(x)\delta(y)\delta(z - z_T), \quad Q = \frac{1}{\mathscr{A}_o}\frac{\partial \mathscr{A}_T}{\partial x}(x), \quad (2.9)$$

where $\mathscr{A}_T(x)$ is the cross-sectional area of the train at distance x from the nose, so that $\mathscr{A}_T(L) \equiv \mathscr{A}_o$, and the ground level line $y = 0$, $z = z_T$ lies in the vertical plane of symmetry of the train. In this case, equation (2.8) becomes

$$p(x, t) \approx \frac{\rho_o U^2 \mathscr{A}_o}{\mathscr{A}} \int Q(x' + U[t]) \frac{\partial \phi^*}{\partial x'}(x', 0, z_T)\, \mathrm{d}x', \quad M^2 \ll 1. \quad (2.10)$$

The source density $Q(x' + U[t])$ is nonzero only in the neighbourhood of $x' \sim -U[t]$ of the retarded position of the train nose. But, $\partial\phi^*/\partial x' \to 1$ when $-x' \gg \sqrt{\mathscr{A}}$ within the tunnel, so that the total pressure rise across the wave predicted by (2.10) is

$$p \sim \frac{\rho_o U^2 \mathscr{A}_o}{\mathscr{A}}, \quad \text{for} \quad U[t] \gg \sqrt{\mathscr{A}}, \quad M^2 \ll 1. \quad (2.11)$$

When the train nose has passed into the tunnel, and no longer interacts with the portal, the pressure rise just ahead of the train is given *exactly* by the Green's function (2.5), wherein now

$$\phi^*(\mathbf{x}) \approx x - \ell', \qquad \phi^*(\mathbf{x}') \approx x' - \ell'.$$

The Mach number restriction on (2.5) can be relaxed provided that only plane waves can propagate in the tunnel (i.e., the wavefront thickness is much larger than the tunnel diameter). In this case equation (2.7) supplies, without approximation, the *constant* pressure ahead of the train (behind the wavefront and before the rear end of the train enters the tunnel) in the form

$$p = \frac{\rho_o U^2}{\mathscr{A}(1-M^2)} \int q(x')\ \mathrm{d}^3\mathbf{x}' = \frac{\rho_o U^2 \mathscr{A}_o}{\mathscr{A}(1-M^2)}, \quad \text{for } U[t] \gg \sqrt{\mathscr{A}}. \tag{2.12}$$

A comparison of this result with equation (2.11) suggests that predictions of the low Mach number formula (2.10) can be extended to finite Mach numbers by writing

$$p(x,t) \approx \frac{\rho_o U^2 \mathscr{A}_o}{(1-M^2)\mathscr{A}} \int Q(x' + U[t]) \frac{\partial \phi^*}{\partial x'}(x', 0, z_T)\, \mathrm{d}x'. \tag{2.13}$$

The validity of this extrapolation formula is discussed below in Section 4.

An overall impression of the influence of tunnel portal geometry on the compression wave profile is obtained by considering the special case of a long train with a profiled nose whose length L tends to zero. For a 'snub' nosed train of this kind the source distribution $q(\mathbf{x})$ of equation (2.9) reduces to a single *point source*, because $Q(x) \equiv (1/\mathscr{A}_o)\partial \mathscr{A}_T/\partial x \to \delta(x)$ as $L \to 0$. The compression wave pressure at low Mach numbers is therefore given by (2.10) by setting $Q(x' + U[t]) = \delta(x' + U[t])$, which yields

$$p(x,t) = \frac{\rho_o U^2 \mathscr{A}_o}{\mathscr{A}} \left(\frac{\partial \phi^*}{\partial x'}(x', 0, z_T) \right) \Bigg|_{x' = -U[t]}, \quad M^2 \ll 1. \tag{2.14}$$

3. THE FLARED PORTAL WHEN $M^2 \ll 1$

3.1. Exact Calculation of $\phi^*(\mathbf{x})$

The function $\phi^*(\mathbf{x})$ that determines the compression wave in equations (2.10) and (2.13) is the solution of Laplace's equation satisfying conditions (2.6), and represents an irrotational flow from the tunnel portal that has unit speed in the uniform section of the tunnel. By introducing the *image* of the tunnel in the ground plane $y = 0$, the calculation of $\phi^*(\mathbf{x})$ is seen to be equivalent to determining irrotational flow from an axisymmetric duct. Indeed, the original problem in Figure 1 of a train entering a tunnel is mathematically the same as that of the train plus its *image* in the ground plane ($y = 0$) entering the duct [cf. Figure 3(a), below].

The following *exact* representation of $\phi^*(\mathbf{x})$ is available when the duct consists of an unflanged, semi-infinite circular cylinder of radius R_0 (Howe 1998a)

$$\phi^*(\mathbf{x}) \equiv \phi^*(x, r), \quad r = \sqrt{y^2 + z^2}, \tag{3.1}$$

where

$$\frac{\partial \phi^*}{\partial x} = \frac{1}{2} - \frac{1}{4\pi} \int_{-\infty}^{\infty} \frac{\mathrm{I}_0(\lambda r/R_0)\sqrt{2\mathrm{K}_1(|\lambda|)\mathrm{I}_1(|\lambda|)}}{\mathrm{I}_1(\lambda)} \sin(\lambda[x/R_0 + \mathscr{F}(\lambda)])\, \mathrm{d}\lambda,$$

$$\mathscr{F}(\lambda) = \frac{1}{\pi} \int_0^{\infty} \frac{\ln[\mathrm{K}_1(\mu)\mathrm{I}_1(\mu)/\mathrm{K}_1(|\lambda|)\mathrm{I}_1(|\lambda|)]}{\mu^2 - \lambda^2}\, \mathrm{d}\mu, \tag{3.2}$$

I_0, I_1, K_0, K_1 are modified Bessel functions, and the coordinate origin is in the exit plane of the cylinder.

The Stokes' stream function $\psi^*(\mathbf{x}) \equiv \psi^*(x, r)$, that assumes constant values on the axisymmetric stream surfaces of the hypothetical flow from the cylinder, is determined in terms of ϕ^* by (Landau & Lifshitz 1987)

$$\frac{\partial \phi^*}{\partial x} = \frac{1}{r}\frac{\partial \psi^*}{\partial r}, \quad \frac{\partial \phi^*}{\partial r} = -\frac{1}{r}\frac{\partial \psi^*}{\partial x}.$$

Figure 2 depicts the stream surface profiles for several constant values of $\Psi^* = 2\pi\psi^*/\pi R_0^2 \equiv 2\psi^*/R_0^2$. These values represent the fraction of the total volume flux from the duct between the stream surface and the x-axis. Any one of these surfaces $\Psi^* = C$, say (where C is a constant between zero and 1) can be replaced by a *rigid boundary*, and the velocity potential ϕ^* may then be interpreted as the potential of flow through a "conically" divergent nozzle whose uniform, asymptotic cross-section as x becomes large and negative is $\mathscr{A} = C\pi R_0^2$, corresponding to a uniform radius $R = R_0\sqrt{C}$.

The stream surface for $C \approx 0{\cdot}507$ defines the boundary of a flared portal with an infinite flange, as illustrated in Figure 3(a) (for which $R \approx 0{\cdot}71R_0$). The corresponding compression wave pressure and pressure "gradient" $\partial p/\partial t$ for a snub nosed train modelled by a point source are determined by equation (2.14), where ϕ^* is given by equation (3.2), and are plotted in Figure 3(b) as functions of the nondimensional retarded time $U[t]/R$ when the source travels along the x-axis. Note that $[t] = t + (x - \ell')/c_o$, where x is measured from an origin O in the plane of the tunnel flange (which does *not* coincide with the entrance plane of the unflanged cylinder of Figure 2). The dotted curve is discussed in Section 3.2. The influence of flaring in this case can be assessed by comparison with the corresponding

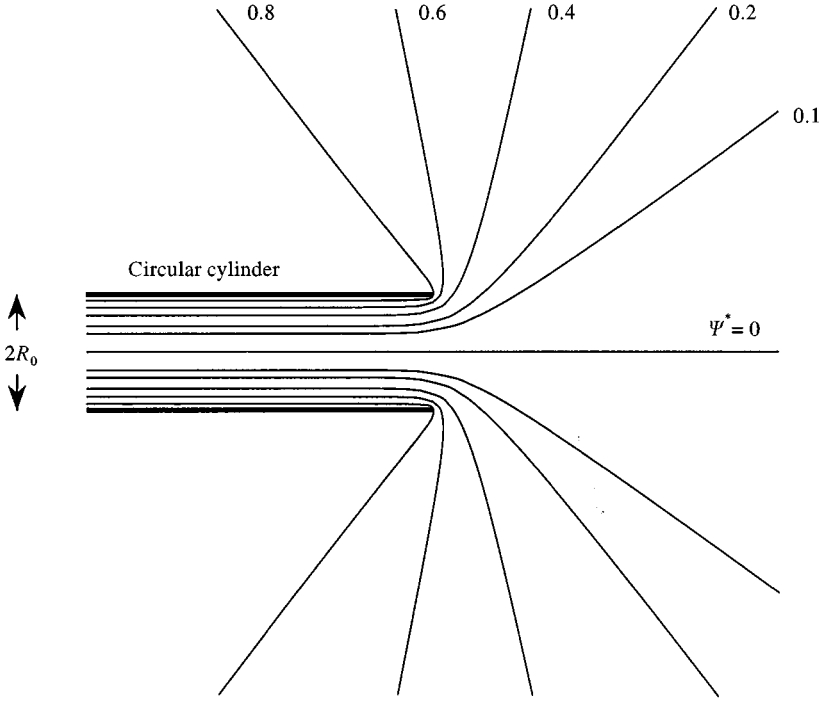

Figure 2. Profiles of the stream surfaces $\Psi^* = 2\psi^*/R_0^2 =$ constant, for uniform potential flow from a circular cylindrical duct of radius R_0.

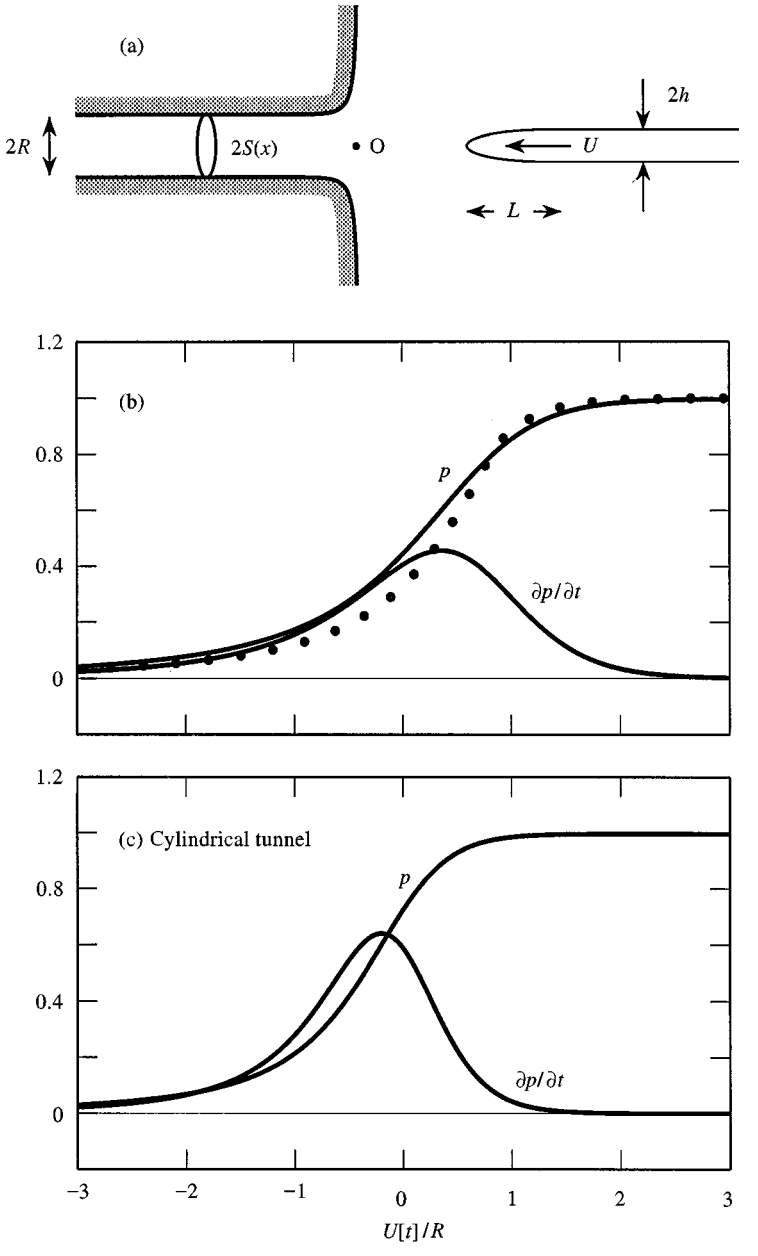

Figure 3. (a) Axisymmetric flanged portal defined by the stream surface $\Psi^* = 0{\cdot}507$ of Figure 2. (b) Nondimensional pressure $p/(\rho_o U^2 \mathscr{A}_o/\mathscr{A})$ and pressure "gradient" $(\partial p/\partial t)/(\rho_o U^3 \mathscr{A}_o/\mathscr{A}R)$ for a snub-nosed train when $M^2 \ll 1$; the dotted curve is discussed at the end of Section 3.2. (c) Corresponding pressure and pressure gradient for a uniform (unflanged) duct entrance of radius R.

pressure and pressure gradient depicted in Figure 3(c) for the unflanged circular cylinder (corresponding to $C = 1$ and $R = R_0$), where the absence of flange and the presence of the sharp edged opening produce a compression wave whose thickness is about R/M smaller, where R is the common internal radius of both tunnels.

3.2. Approximate Calculation of $\phi^*(\mathbf{x})$

Consider next a flared axisymmetric duct whose cross-sectional area, $2S(x)$ (Figure 4) changes slowly over distances of the order of the duct radius. The axial velocity $\partial\phi^*(\mathbf{x})/\partial x$ is approximately constant over any cross-section, and Laplace's equation for ϕ^* reduces to the ordinary differential equation (Landau & Lifshitz 1987)

$$\frac{1}{S(x)}\frac{\partial}{\partial x}\left(S(x)\frac{\partial\phi^*}{\partial x}\right) = 0, \quad x < 0. \tag{3.3}$$

The solution satisfying equation (2.6) is readily found in the form

$$\phi^*(\mathbf{x}) = \mathscr{A}\int_0^x \frac{\mathrm{d}\xi}{S(\xi)} + \alpha, \quad x < 0, \tag{3.4}$$

where α is a constant, in terms of which the end-correction is given by

$$\ell' = -\alpha + \int_{-\infty}^{0}\left(\frac{\mathscr{A}}{S(\xi)} - 1\right)\mathrm{d}\xi. \tag{3.5}$$

The value of α depends on the behaviour of $\phi^*(\mathbf{x})$ outside the tunnel portal ($x > 0$). For the purpose of this calculation, it will be assumed that the duct terminates in an infinite *flange* (see Figure 4), in which case the potential in the exterior region is given by (Morse & Feshbach 1953)

$$\phi^*(x) = -\frac{1}{2\pi}\int_{\mathscr{A}_E}\frac{u(y', z')\,\mathrm{d}y'\,\mathrm{d}z'}{\sqrt{(x^2 + (y - y')^2 + (z - z')^2}}, \quad x > 0, \tag{3.6}$$

where the integration is over the duct exit. In this formula,

$$u(y, z) = u_o \equiv \left(\frac{\partial\phi^*}{\partial x}\right)_{x=0}, \tag{3.7}$$

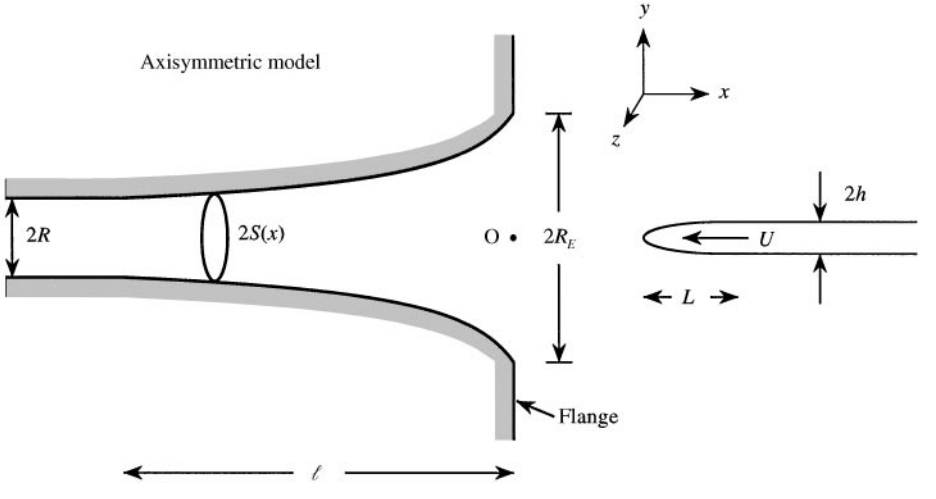

Figure 4. Axisymmetric flared portal with infinite flange.

which, according to equation (3.4), is constant and equal to $\mathscr{A}/\mathscr{A}_E$ over the duct exit. Then, on the axis of symmetry,

$$\phi^*(\mathbf{x}) = -\frac{\mathscr{A}R}{\mathscr{A}_E}\left[\left(\frac{\mathscr{A}_E}{\mathscr{A}} + \frac{x^2}{R^2}\right)^{1/2} - \frac{x}{R}\right], \quad x > 0, \tag{3.8}$$

and continuity supplies

$$\alpha = -R\sqrt{\frac{\mathscr{A}}{\mathscr{A}_E}}. \tag{3.9}$$

The integral definition of $\phi^*(\mathbf{x})$ outside the tunnel can be used to evaluate $\phi^*(\mathbf{x})$ everywhere in $x > 0$, but the general formula will not be needed in the present discussion, where attention will be confined to trains travelling along the axis of symmetry.

The validity of the approximation (3.4) for ϕ^* can be investigated by considering first the flared portal illustrated in Figure 5(a). The duct wall to the left of the exit plane corresponds to that member of the family of stream surfaces in Figure 2 for which $\Psi^* = 0{\cdot}06$, and the location of the exit plane ($x = 0$) has been adjusted to make $\mathscr{A}/\mathscr{A}_E = 0{\cdot}06$ (so that $R_E = R_0$, and $R/R_E \approx 0{\cdot}25$). The solid curves in Figure 5(b) represent the pressure and pressure gradient calculated from equation (2.14) during the time in which a train modelled by

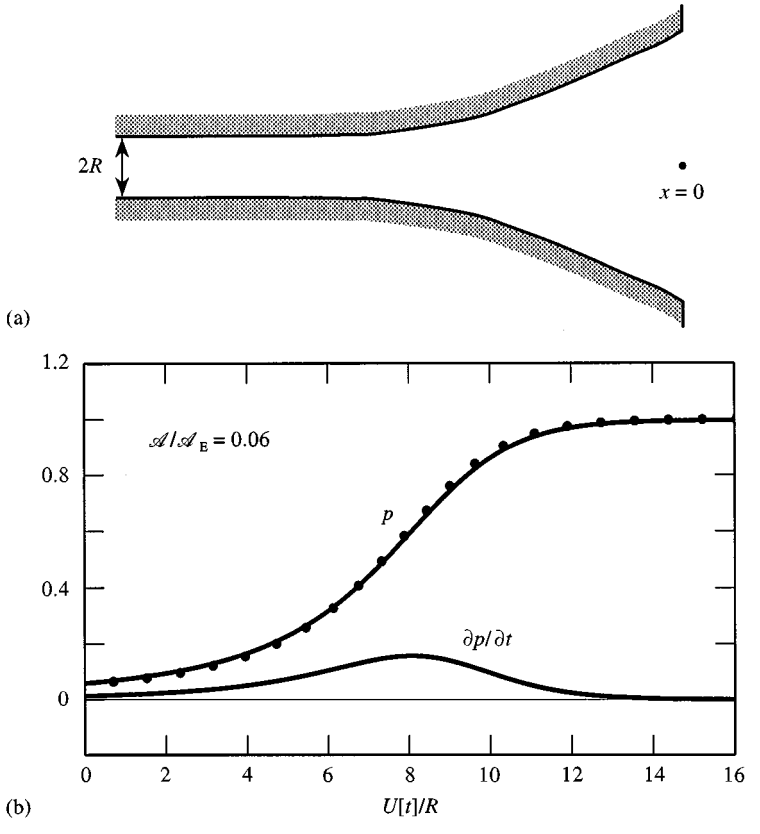

Figure 5. (a) Axisymmetric portal determined by the stream surface $\Psi^* = 0{\cdot}06$ in Figure 2. (b) Nondimensional pressure $p/(\rho_o U^2 \mathscr{A}_o/\mathscr{A})$ and pressure "gradient" $(\partial p/\partial t)/(\rho_o U^3 \mathscr{A}_o/\mathscr{A}R)$ for a point source entering the tunnel when $M^2 \ll 1$. The dotted curve is the pressure calculated using approximation (3.4).

a point source is within the flared section and translates along the axis of symmetry, as in Section 3.1, when $\phi^*(\mathbf{x})$ is given by the exact formula (3.2) for flow through a conical nozzle.

The dotted curve in Figure 5(b) is the pressure determined for the same time interval by the approximation (3.4) for ϕ^*, which, from eqution (2.14) gives the pressure in the form

$$p(x, t) = \frac{\rho_o U^2 \mathscr{A}_o}{S(-U[t])}, \quad \text{for } U[t]/R > 0, \tag{3.10}$$

where $2S(x)$ is the cross-sectional area of the stream tube $\Psi^* = 0{\cdot}06$ at distance $|x|$ into the tunnel. The agreement between the exact and approximate predictions is excellent.

However, there is a substantial error in applying equation (3.4) to the flanged portal of Figure 3(a) [which yields the dotted curve in Figure 3(b)]. The approximation is invalid at distances less than about $0{\cdot}64R$ from the exit plane, so that the prediction (3.10) is correct only for $U[t]/R$ greater than about 0·64. The dotted curve in Figure 3(b) has been estimated for $U[t]/R < 0{\cdot}64$ by applying the piston approximation (3.8) in $x > -0{\cdot}64R$, where $2\mathscr{A}_E$ is the portal cross-section at $x = -0{\cdot}64R$.

3.3. Optimal Flaring when $M^2 \ll 1$

To maximize the initial compression wave rise time the duct cross-section must necessarily vary slowly with axial distance x, and the approximation (3.4) should therefore be applicable. For a snub-nosed train, modelled by a point source, the compression wave profile is therefore given by equation (3.10) at retarded times when the train is within the flared section, where most of the pressure rise occurs. The retarded cross section $S(-U[t])$ decreases from $\mathscr{A}_E$ to $\mathscr{A}$ during this time, so that the pressure rises from $\rho_o U^2 \mathscr{A}_o/\mathscr{A}_E$ when the front of the train (the source) is just entering the tunnel, to its final value of $\rho_o U^2 \mathscr{A}_o/\mathscr{A}$, when the front enters the uniform section of the tunnel. This increase will occur uniformly if the inverse cross-section $1/S(-U[t])$ increases *linearly* with time, that is, provided the tunnel flaring is defined by

$$\frac{S(x)}{\mathscr{A}} = \frac{1}{[\mathscr{A}/\mathscr{A}_E - (x/\ell)(1 - \mathscr{A}/\mathscr{A}_E)]}, \quad -\ell < x < 0. \tag{3.11}$$

The tunnel radius $r(x) = R\sqrt{S(x)/\mathscr{A}}$, and the profiles shown in Figures 1 and 4 are determined by this formula when $\ell/R = 10$ and $\mathscr{A}/\mathscr{A}_E = 0{\cdot}1$.

However, for an arbitrarily chosen value of $\mathscr{A}/\mathscr{A}_E$ the retarded value of the predicted pressure gradient will generally be discontinuous at the entrance plane ($U[t]/R = 0$) where the definition of $\phi^*(\mathbf{x})$ changes from equation (3.4) to (3.8). Thus, when the length ℓ of the flared section has been prescribed, the shape of the optimally flared portal is obtained by adjusting the value of $\mathscr{A}/\mathscr{A}_E$ in equation (3.11) to ensure that the pressure varies smoothly at $U[t]/R = 0$. This is equivalent to requiring $\partial^2\phi^*(x, 0, 0)/\partial x^2$ to be continuous across the tunnel entrance plane $x = 0$. By using the formulae (3.4), (3.8), which are respectively valid for $x \lesseqgtr 0$, this condition is easily seen to require that

$$\left(\frac{\mathscr{A}}{\mathscr{A}_E}\right)^{3/2} = \frac{R}{\ell}\left(1 - \frac{\mathscr{A}}{\mathscr{A}_E}\right), \tag{3.12}$$

i.e. (for $R/\ell < 3\sqrt{3}/2 \approx 2{\cdot}6$)

$$\frac{\mathscr{A}}{\mathscr{A}_E} = \frac{(2R/\ell)^{2/3}}{\left[\left(1 + \sqrt{1 - \left(\frac{2R}{3\sqrt{3}\ell}\right)^2}\right)^{1/3} + \left(1 - \sqrt{1 - \left(\frac{2R}{3\sqrt{3}\ell}\right)^2}\right)^{1/3}\right]^2}. \tag{3.13}$$

According to this formula, $\mathscr{A}/\mathscr{A}_E$ increases smoothly from zero to $\frac{3}{4}$ as R/ℓ increases from zero to 2·6.

For the particular case in which $\ell/R = 10$, equation (3.13) gives $\mathscr{A}/\mathscr{A}_E \approx 0{\cdot}187$, so that the tunnel entrance radius $R_E \approx 2{\cdot}3R$. The corresponding calculated linear pressure rise across the wavefront is illustrated in Figure 6 as a function of $U[t]/R$, the nondimensional retarded position of the front of the train (the point source). The pressure for $U[t]/R < 0$, before the train enters the flared portal, is calculated from (2.14) (with $z_T = 0$) by taking $\phi^*(\mathbf{x})$ to be given by the piston approximation (3.8). The pressure increases uniformly as the source traverses the flared section of length $10R$, producing a compression wave thickness $\sim 10R/M \gg R$. The "pressure gradient" $\partial p/\partial t$ (also plotted in the figure) rises to a small and constant value as the train enters the flared portal.

The optimal prediction of Figure 6 should be contrasted with the prediction in Figure 5, where a similar increase in wave thickness is achieved using a "conically" flared portal. The rise in pressure across the wavefront is not linear for the conical portal; the pressure gradient $\partial p/\partial t$ has a distinct maximum, where the slope of the wavefront is about twice that for the optimally flared portal of roughly the same effective length ℓ. Furthermore, the somewhat more modest improvements in the compression wave profile achieved by conical flaring require the exit radius $R_E = R/\sqrt{0{\cdot}06} \approx 4{\cdot}1R$, nearly twice that of the optimally flared portal.

4. PREDICTIONS AT FINITE MACH NUMBER

4.1. Extrapolation to Higher Mach Numbers

For a snub-nosed train (equivalent to a point source) entering an unflanged circular cylindrical tunnel of radius R along the axis of symmetry, the peak pressure gradient at mach number M was shown by Howe (1998b) to be given by

$$\left(\frac{\partial p}{\partial t}\right)_{\max} = \left(\frac{\rho_o U^3 \mathscr{A}_o}{R\mathscr{A}}\right)\frac{0{\cdot}64 + 1{\cdot}3M^6}{1 - M^2}, \quad 0 < M < 0{\cdot}6. \tag{4.1}$$

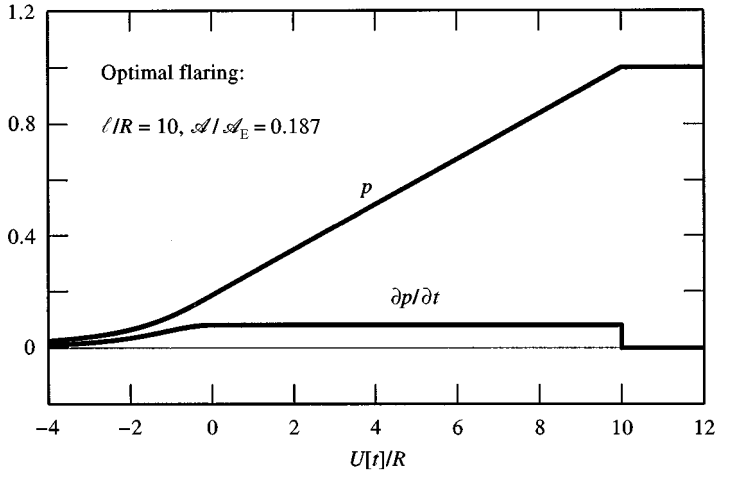

Figure 6. Nondimensional pressure $p/(\rho_o U^2 \mathscr{A}_o/\mathscr{A})$ and pressure "gradient" $(\partial p/\partial t)/(\rho_o U^3 \mathscr{A}_o/\mathscr{A}R)$ for a snub-nosed train entering an optimally flared portal of the type shown in Figure 4 when $\ell/R = 10$, $\mathscr{A}/\mathscr{A}_E = 0{\cdot}187$ and $M^2 \ll 1$.

This formula was derived from equation (2.3) by using the *exact* Green's function [solution of (2.4)] for the unflanged circular cylinder [equation (9) of Howe 1998b]. The error incurred in omitting the term in M^6 is less than 1% when $M \leq 0{\cdot}4$.

Exact predictions for this case of p and $\partial p/\partial t$ as functions of the retarded time $U[t]/R = 0$ for $M = 0{\cdot}1, 0{\cdot}2, 0{\cdot}3, 0{\cdot}4$ are displayed in Figure 7(a). The corresponding predictions of the extrapolation formula (2.13) for the same Mach numbers are shown in Figure 7(b), for which

$$p(x, t) = \frac{\rho_o U^2 \mathscr{A}_o}{\mathscr{A}(1 - M^2)} \left(\frac{\partial \phi^*}{\partial x'} (x', 0, 0) \right)_{x' = -U[t]}, \tag{4.2}$$

where $\partial \phi^*(\mathbf{x})/\partial x$ is given by equation (3.2) with $R_0 = R$. The exact and approximate results differ by a small *phase shift*; when this is removed, the corresponding pressure and pressure gradient curves are in excellent accord. For the purpose of optimizing portal design, small phase errors of this kind are of no practical significance.

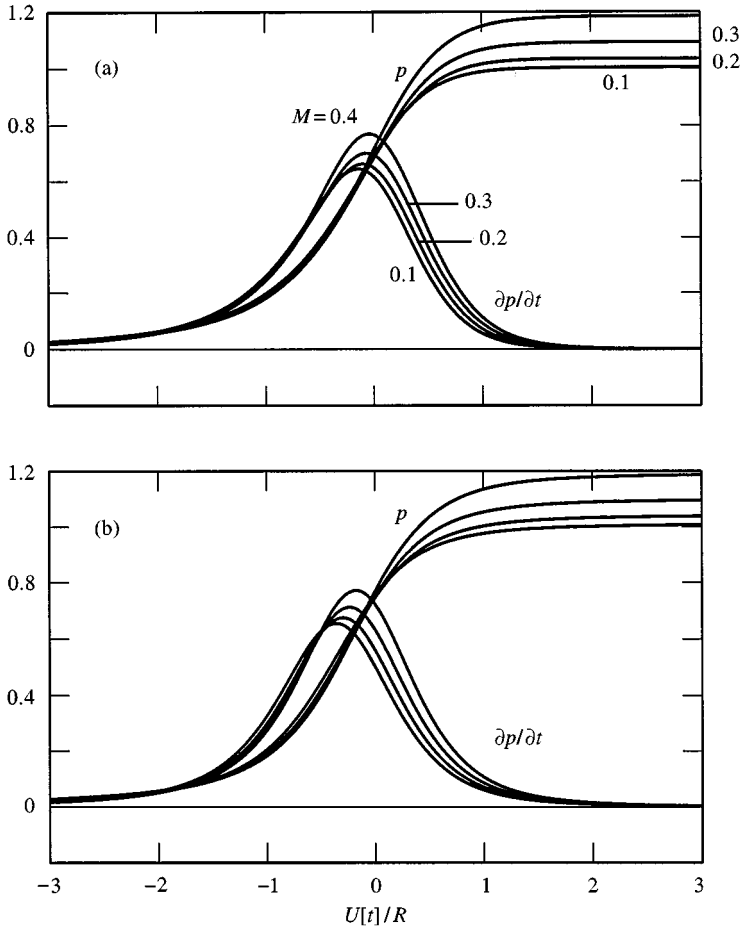

Figure 7. Nondimensional pressure $p/(\rho_o U^2 \mathscr{A}_o/\mathscr{A})$ and pressure "gradient" $(\partial p/\partial t)/(\rho_o U^3 \mathscr{A}_o/\mathscr{A}R)$ for a snub-nosed train entering a circular cylindrical tunnel of radius R at different Mach numbers: (a) calculated by Howe (1998b) using the exact Green's function; (b) calculated from the extrapolation formula (4.2) using (3.2).

Indeed such discrepancies are hardly noticeable when predictions of these formulae are compared with experiment. This is well illustrated by the data of Maeda *et al.* (1993), obtained using axisymmetric, wire-guided model "trains" projected along the axis of a 7 m long, unflanged circular cylinder of radius $R = 0{\cdot}0735$ m. The nose profiles (of length L) included the cone, and the paraboloid and ellipsoid of revolution [see column (a) of Figure 8] with respective cross-sectional areas

$$\frac{\mathscr{A}_T(x)}{\mathscr{A}_o} = \begin{cases} \dfrac{x^2}{L^2}, \ \dfrac{x}{L}, \ \dfrac{x}{L}\left(2 - \dfrac{x}{L}\right), & 0 < x < L, \\ 1, & x \geq L, \end{cases} \tag{4.3}$$

where x is measured from the tip of the nose. The corresponding source densities Q of equation (2.9) are

$$Q(x) = \begin{cases} \dfrac{2x}{L^2}, \ \dfrac{1}{L}, \ \dfrac{2}{L}\left(1 - \dfrac{x}{L}\right), & 0 < x < L, \\ 0, & \text{elsewhere}, \end{cases} \tag{4.4}$$

and are plotted in column (b) of Figure 8.

The data from these experiments plotted in Figure 9 are values of the pressure gradient $\partial p/\partial t$ measured within the cylinder at 1 m from the entrance plane. The trains had aspect ratio $h/L = 0{\cdot}2$, where h is the uniform cross-sectional radius of a train to the rear of the nose (so that $\mathscr{A}_o = \pi h^2$) and area ratio $\mathscr{A}_o/\mathscr{A} = 0{\cdot}116$, and were projected axisymmetrically

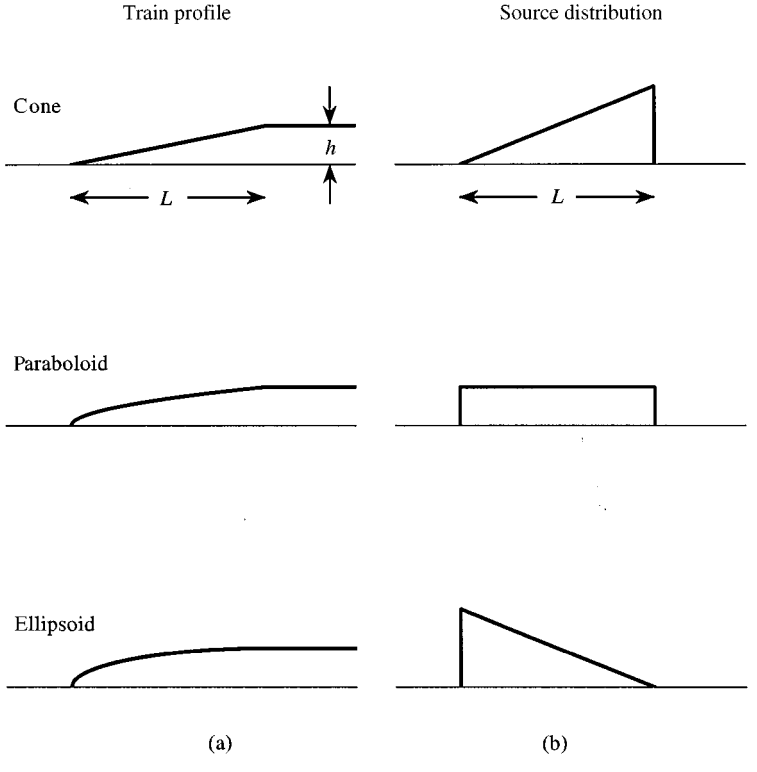

Figure 8. (a) Train profiles and (b) source distributions for the axisymmetric experimental trains.

into the cylinder at $U = 230$ km/h ($M = 0{\cdot}188$). The solid curves in Figure 9(a) represent predictions of equations (2.3) and (2.9) using the *exact* Green's function and the source densities (4.4). The predicted peak values of $\partial p/\partial t$ are just under 5% *smaller* than the corresponding measurements. In plotting these curves, the retarded time origin has been shifted so that the peaks for theory and experiment coincide for the *ellipsoid*. This adjustment gives excellent overall agreement for all three cases.

Figure 9(b) shows the same comparison with experiment of predictions of the extrapolation formula (2.13) when the velocity potential ϕ^* is given by equation (3.2). The evident effective agreement of the exact and approximate theories lends strong support to the validity of the extrapolation procedure for *any* tunnel portal geometry provided the compression wave thickness is large compared to the relevant length ℓ that characterizes the extent of the variable section of the tunnel portal. When this latter condition is satisfied the *physical* basis of the compact approximation is the same as it is for the circular cylindrical portal.

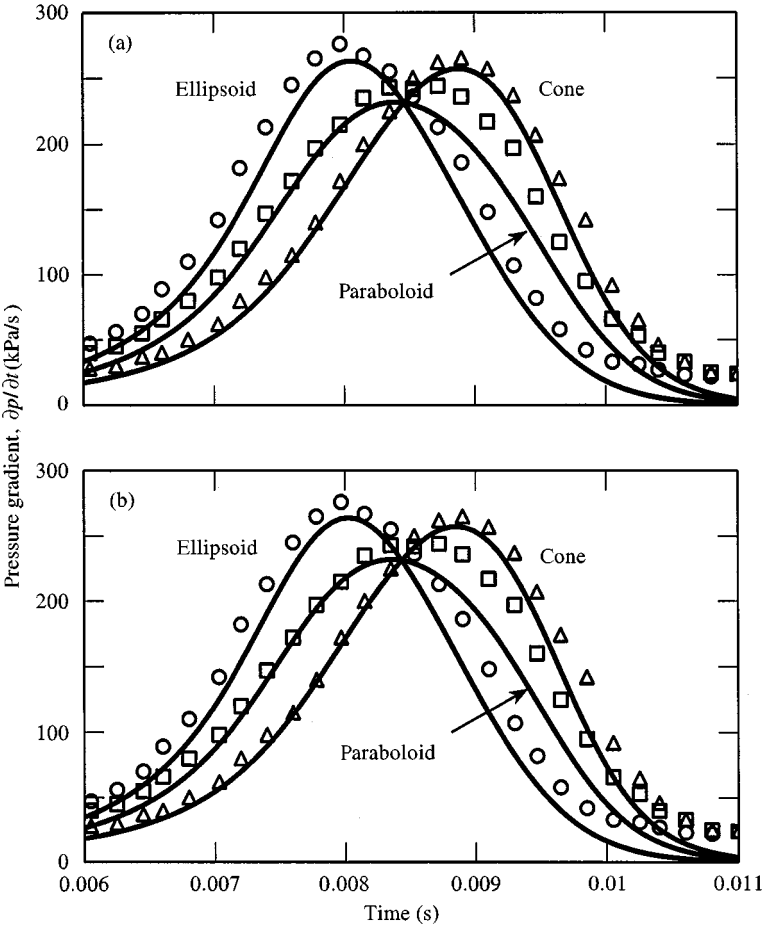

Figure 9. Comparison of the predicted pressure "gradient" $\partial p/\partial t$ (solid curves) with measurements of Maeda *et al.* (1993) for axisymmetric model trains entering a circular cylindrical 'tunnel' at $M = 0{\cdot}188$: (a) calculated by Howe (1998b) using the exact Green's function; (b) calculated from the extrapolation formula (2.13) using equation (3.2).

4.2. The Optimally Flared Portal

Consider the application of the extrapolation formula (2.13) to a flared portal, when $\phi^*(\mathbf{x})$ is defined by equation (3.4) and the piston approximation (3.8). Figure 10(a) illustrates typical predictions of the compression wave pressure and pressure gradient for the cone, paraboloid and ellipsoid nose profiles defined in equation (4.3) (see Figure 8) for $M = 0{\cdot}4$, $L/R = 2$, for a flared section of length $\ell = 10R$, area ratio $\mathscr{A}/\mathscr{A}_E = 0{\cdot}187$, when

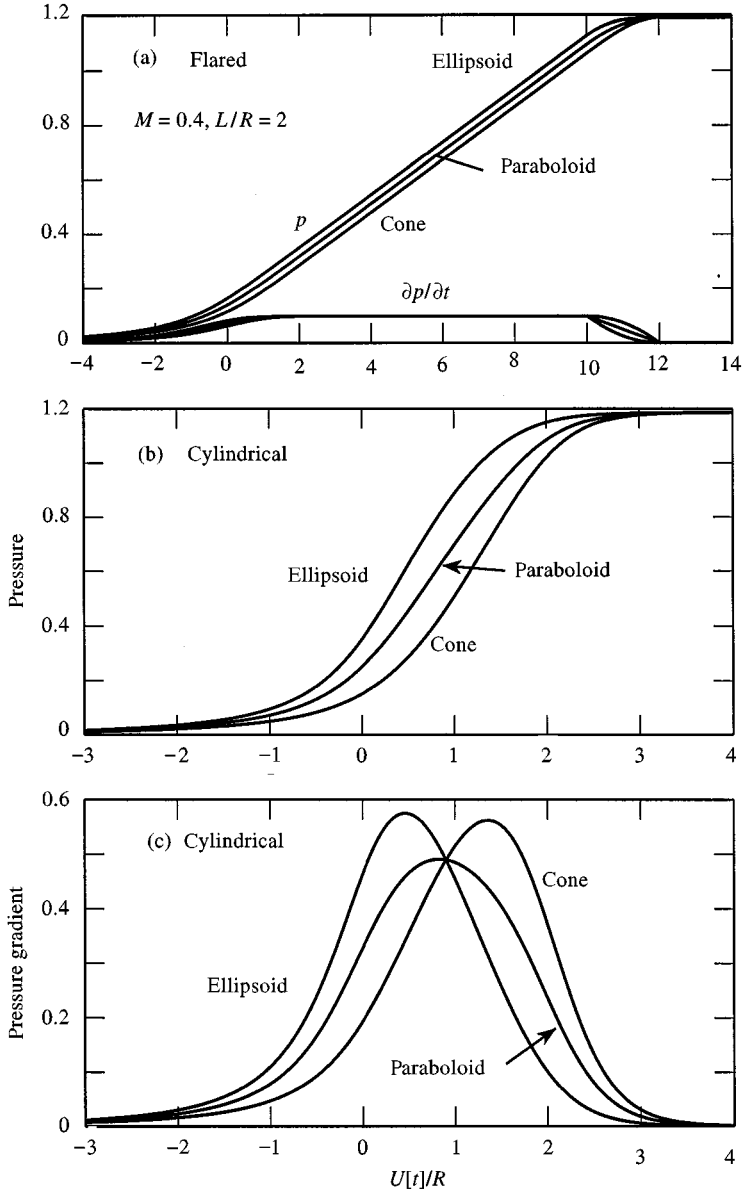

Figure 10. Nondimensional pressure $p/(\rho_o U^2 \mathscr{A}_o/\mathscr{A})$ and pressure "gradient" $(\partial p/\partial t)/(\rho_o U^3 \mathscr{A}_o/\mathscr{A}R)$ for the axisymmetric model trains of Figure 8 for $M = 0{\cdot}4$, $L/R = 2$: (a) optimally flared portal with $\ell/R = 10$, $\mathscr{A}/\mathscr{A}_E = 0{\cdot}187$; (b), (c) corresponding profiles for a tunnel in the form of an unflanged circular cylindrical duct of radius R.

the tunnel portal is optimally flared in accordance with equations (3.11) and (3.13). The predicted pressure profiles are smooth everywhere, in contrast to the prediction in Figure 6 for a snub-nosed train. This is because the source density Q is now distributed over the finite length L of the profiled nose. All of the pressure curves are qualitatively similar: each is dominated by a long interval $0 < U[t]/R < 12$ of essentially *linear* growth occurring as the nose passes through the flared section, such that the compression wave thickness $\sim 12R/M = 30R$.

Figure 10(b, c) illustrates the predicted pressure and pressure gradient profiles for a non-flared, unflanged cylindrical tunnel [taken from Howe's (1998b) paper, which made use of the exact Green's function for the cylinder] at the same Mach number. The wave thickness is here $\sim 3R/M = 7{\cdot}5R$, and the maximum pressure gradient is about five times larger than for the flared portal.

5. CONCLUSION

The structure of the compression wave generated by a high-speed train entering a tunnel depends critically on tunnel portal geometry. The wave amplitude increases approximately as M^2 for a train travelling at Mach number M, and the initial compression wave thickness decreases like $1/M$; both effects tend to exacerbate nonlinear wave steepening in a long tunnel, and the environmental damage produced by the pulsatile radiation of the associated micropressure wave from the distant tunnel exit. The initial wave thickness is increased when the tunnel entrance portal is flared. Flaring produces an optimal compression waveform when the pressure rises *linearly* across the wavefront, so that the pressure gradient is effectively constant (and an overall minimum) within the wavefront. This has, been shown to occur when the tunnel cross-sectional area varies according to equation (3.11) in the flared section, and when the area ratio $\mathscr{A}/\mathscr{A}_E$ is determined by equation (3.13). In this case, the wave thickness $\sim \ell/M$, where ℓ is the length of the flared section.

Detailed analyses have been made for small Mach numbers ($M^2 \ll 1$) , and an extrapolation formula has been proposed that extends predictions to train Mach numbers as large as 0·4. The extrapolation formula has been justified by comparison with exact theoretical results for a tunnel consisting of an unflanged, circular cylinder, and by comparison with model scale experiments for this case performed by Maeda *et al.* (1993).

References

Howe, M. S. 1998a The compression wave produced by a high-speed train entering a tunnel. *Proceedings of the Royal Society* **A454,** 1523–1534.

Howe, M. S. 1998b Mach number dependence of the compression wave generated by a high-speed train entering a tunnel. *Journal of Sound and Vibration* **212,** 23–36.

Iida, M., Matsumura, T., Nakatani, K., Fukuda, T. & Maeda, T. 1996 Optimum nose shape for reducing tunnel sonic boom. Institution of Mechanical Engineers Paper C514/015/96.

Landau, L. D. & Lifshitz, E. M. 1987 *Fluid Mechanics*, second edition. Oxford: Pergamon.

Maeda, T., Matsumura, T., Iida, M., Nakatani, K. & Uchida, K. 1993 Effect of shape of train nose on compression wave generated by train entering tunnel. In *Proceedings of the International Conference on Speedup Technology for Railway and Maglev Vehicles* Yokohama, Japan, 22–26 November, pp. 315–319.

Mestreau, E., Lohner, R. & Aita, S. 1993 TGV tunnel entry simulations using a finite element code with automatic remeshing. AIAA Paper 93-0890.

Morse, P. M. & Feshbach, H. 1953 *Methods of Theoretical Physics*, Vols. 1 and 2. New York: McGraw-Hill.

Ogawa, T. & Fujii, K. 1994a Numerical simulation of compressible flows induced by a train moving into a tunnel. *Computational Fluid Dynamics Journal* **3,** 63–82.

Ogawa, T. & Fujii, K. 1994b Effect of train shape on a compression wave generated by a train moving into a tunnel. In *Proceedings of the Shock Wave Symposium*, Chiba, Japan, sponsored by the Japan Society of Shock Wave Research, the Institute of Fluid Science at Tohoku University, and The Institute of Space and Astronautical Science, January 1994.

Ogawa, T. & Fujii, K. 1996 Prediction and alleviation of a booming noise created by a high-speed train moving into a tunnel. In *Proceedings of the European Community Conference on Computational Methods in Applied Sciences* New York: John Wiley & Sons.

Ogawa, T. & Fujii, K. 1997 Numerical investigation of three dimensional compressible flows induced by a train moving into a tunnel. *Journal of Computers and Fluids* **26,** 565–585.

Ozawa, S., Tsukamoto, K. & Maeda, T. 1976 Model experiments on devices to reduce pressure wave radiated from a tunnel (in Japanese). Railway Technical Research Institute, Japanese National Railways, Report No. 990.

Ozawa, S., Maeda, T., Matsumura, T., Uchida, K., Kajiyama, H. & Tanemoto, K. 1991 Countermeasures to reduce micro-pressure waves radiating from exits of Shinkansen tunnels. In *Aerodynamics and Ventilation of Vehicle Tunnels*, Elsevier Science Publishers, pp. 253–266.

Rayleigh, Lord 1926 *The Theory of Sound*, Volume 2. London: Macmillan.

Swarden, M. C. & Wilson, D. G. 1970 Vehicle-tunnel entry at subsonic speeds. Final Report - Part 1. Rept No. DSR 76111-3, Engineering Projects Laboratory, Department of Mechanical Engineering, Massachusetts Institute of Technology, Cambridge, MA, U.S.A.

Vardy, A. E. 1978 Reflection of step-wavefronts from perforated and flared extensions. *Journal of Sound and Vibration* **59,** 577–589.